Neutron diffraction study of the magnetic ordering in the series R$_2$BaNiO$_5$ (R = Rare Earth)

E. García-Matres[1,a], J.L Martínez[2], and J. Rodríguez-Carvajal[3,b]

[1] Institut Laue-Langevin, BP 156, 38042, Grenoble Cedex, France
[2] Instituto de Ciencia de Materiales (CSIC), Fac. Ciencias (C-4), Universidad Autónoma de Madrid, 28049 Madrid, Spain
[3] Laboratoire Léon Brillouin (CEA-CNRS), Centre d'Études de Saclay, 91191 Gif-sur-Yvette Cedex, France

Abstract. A neutron diffraction study, as a function of temperature, of the title compounds is presented. The whole family (space group Immm, $a \approx 3.8$ Å, $b \approx 5.8$ Å, $c \approx 11.3$ Å) is structurally characterised by the presence of flattened NiO$_6$ octahedra that form chains along the a-axis, giving rise to a strong Ni-O-Ni antiferromagnetic interaction. Whereas for Y-compound only strong 1D correlations exist above 1.5 K, presenting the Haldane gap characteristic of 1D AF chain with integer spin, 3D AF ordering is established simultaneously for both R and Ni sublattices at temperatures depending on the rare earth size and magnetic moment. The magnetic structures of R$_2$BaNiO$_5$ (R = Nd, Tb, Dy, Ho, Er and Tm) have been determined and refined as a function of temperature. The whole family orders with a magnetic structure characterised by the temperature-independent propagation vector **k** = (1/2, 0, 1/2). At 1.5 K the directions of the magnetic moments differ because of the different anisotropy of the rare earth ions. Except for Tm and Yb (which does not order above 1.5 K), the magnetic moment of the R^{3+} cations are close to the free-ion value. The magnetic moment of Ni^{2+} is around 1.4 μ_B, the strong reduction with respect to the free-ion value is probably due to a combination of low-dimensional quantum effects and covalency. The thermal evolution of the magnetic structures from T_N down to 1.5 K is studied in detail. A smooth re-orientation, governed by the magnetic anisotropy of R^{3+}, seems to occur below and very close to T_N in some of these compounds: the Ni moment rotates from nearly parallel to the a-axis toward the c-axis following the R moments. We demonstrate that for setting up the 3D magnetic ordering the R-R exchange interactions cannot be neglected.

PACS. 61.12.-q Neutron diffraction and scattering – 61.66.Fn Inorganic compounds – 75.25.+z Spin arrangements in magnetically ordered materials (including neutron and spin-polarized electron studies, synchrotron-source x-ray scattering, etc.) – 75.30.Et Exchange and superexchange interactions

Introduction

Since the discovery of high T_c-superconductivity in copper oxides, the regain of interest in oxides has stimulated a large amount of theoretical and experimental work in the field of the electronic and magnetic properties of the so called "charge transfer" insulators. Many Ni-oxides seem to belong to this category of insulators. In the last years several neutron scattering studies have been devoted to the investigation of layered perovskite-related nickelates (Ln$_2$NiO$_{4+\delta}$, Ln$_{2-x}$Sr$_x$NiO$_{4+\delta}$; Ln: La, Pr, Nd) presenting 2D structural and magnetic features [1,2], as well as to the metal-insulator transition in the 3D-RNiO$_3$ perovskites (R = Pr, Nd) [3].

The R$_2$BaNiO$_5$ (R = Rare earth or Y) oxides present interesting structural and magnetic properties due to the fact that their structure posses a strong 1D character [4,5]. These oxides crystallise in the orthorhombic system, S.G. Immm, having approximate cell parameters $a \approx 3.8$ Å, $b \approx 5.8$ Å, $c \approx 11.3$ Å. The main structural feature is the presence of one-dimensional (1D) chains of NiO$_6$ octahedra along the a-axis. The octahedra are strongly distorted with a very short Ni-O$_{apical}$ distance (≈ 1.88 Å), and a longer Ni-O$_{basal}$ distance (≈ 2.18 Å). Moreover the basal angle O-Ni-O ($\approx 78°$) is also much smaller than expected for a regular octahedron (90°). The structural details at room temperature and the dependence of the rare earth size upon the structural parameters have been extensively discussed in a previous paper [6].

It is known that the compounds with the heaviest rare earth ions (Tm, Yb and Lu) are dimorphic [7]. The second type of structure is isomorphous to the so called "green

[a] *Present address*: Hahn-Meitner-Institut Glienicker Strasse 100, 14109 Berlin
[b] e-mail: juan@llb.saclay.cea.fr

phases" R_2BaCuO_5 (space group Pnma) which appear as impurities in the synthesis of 123-compounds. In this second phase the Ni-ions are five-fold oxygen-coordinated in isolated square pyramids. In order to study the magnetic properties of this phase, neutron diffraction measurements have been performed and 3D-magnetic ordering has not been observed above 1.5 K. For that reason, in the present paper, the magnetic structure study will be devoted only to the Immm-compounds.

As a consequence of the crystal structure, these compounds are candidates to present low dimensional magnetic properties. Direct oxygen bonds between chains are absent, so the chains are magnetically linked through the R^{3+} and Ba^{2+} ions. The most remarkable low dimensionality behaviour is effectively observed for Y_2BaNiO_5, in which the chains are linked only by diamagnetic cations Ba^{2+} and Y^{3+}. Because of that, the magnetic interchain interactions are very weak and the compound behaves as a nearly pure 1D antiferromagnetic system without 3D antiferromagnetic ordering above 1.5 K. This behaviour is clearly observed in magnetic susceptibility and neutron diffraction measurements. In fact, the Y_2BaNiO_5 compound can be considered as a prototype of the 1D Heisenberg antiferromagnet with $S = 1$. The Haldane gap for $S = 1$ has been observed by means of inelastic neutron scattering [8,9].

The introduction of paramagnetic rare earth ions modifies the magnetic behaviour of R_2BaNiO_5 and 3D magnetic order is observed. Up to now only the magnetic structure of Er, Ho, Pr and Nd compounds have been reported [10–13]. These compounds are antiferromagnetic with propagation vector $\mathbf{k} = (1/2, 0, 1/2)$, however the directions of magnetic moments are different as a consequence of the different anisotropy of the two rare earth ions.

Macroscopic magnetic measurements on these compounds have been performed by different groups. The value of the Néel temperature T_N differs from the temperature of the maximum observed in the magnetic susceptibility [14]. This behaviour can be explained with a simple molecular field model [15,16] and it is not related to oxygen stoichiometry as suggested in [13]. It is interesting to point out that R_2BaNiO_5 (R = Nd, Gd, Tb, Dy, Ho, Er, Tm) oxides present metamagnetic transitions at 4.2 K for magnetic fields between 13 kOe to 180 kOe [15,16].

In the present paper we present the low temperature neutron diffraction experiments carried out for the whole set of the magnetic rare earth compounds of this family (R = Nd, Dy, Tb, Ho, Er, Tm, Yb and Y). Only those compounds where the absorption of neutrons is too strong (Sm, Eu, Gd) have not been studied yet. We have found that the whole series orders with the same propagation vector $\mathbf{k} = (1/2, 0, 1/2)$ and at relatively high temperature: between 15 K to 61 K depending on the rare earth ions.

The aim of the present article is to compare the magnetic ordering of the Immm-R_2BaNiO_5 compounds and discuss, qualitatively, their common features. A discussion of their macroscopic magnetic properties can be found

in [16]. An analysis of the microscopic magnetic interactions responsible for the particular magnetic ordering observed in this series is presented.

Experimental

R_2BaNiO_5 oxides were prepared as polycrystalline samples by solid state reaction from stoichiometric high purity oxides R_2O_3 (99.999%) $BaCO_3$ (Reactive for Analysis grade) and NiO (99.999%) by heating in air at 1200 °C for 48 hours, with several interruptions for grinding.

Neutron diffraction data were obtained in the medium-resolution powder diffractometer D1B at the High-Flux Reactor of the Institut Laue-Langevin (ILL, Grenoble, France). The diffractometer D1B is equipped with a Position Sensitive Detector (PSD) covering an angular range of 80° (2θ) and working at $\lambda = 2.52$ Å. The PSD is composed of 400 sensitive elements separated by 0.2° (2θ). For Tb and Nd oxides, the experiments were carried out on the diffractometer D1A at Laboratoire Léon Brillouin (LLB, Saclay, France). The diffractometer D1A, at Saclay for the period of refurbishment of the ILL reactor, was installed in the position G4.2 of a cold neutron guide. The wavelength used was 2.58 Å from the Ge-(004) reflection. The contamination with $\lambda/2$ harmonic is lower than 0.15% in integrated intensity. In all cases, standard orange He cryostats were used in the temperature range between 1.5 K and room temperature.

All the data were analysed with the Rietveld method using the FULLPROF program [17]. The background was fitted to a polynomial function and the lineshape of peaks was considered as pseudo-Voigt functions with predominant Gaussian component. The magnetic form factors ($f(Q) = \langle j_0 \rangle + c_2 \langle j_2 \rangle$) were calculated from the approximation for $\langle j_\lambda \rangle$ (linear combination of exponential functions of the square of the scattering vector) given in [18]. For Ni^{2+}, only the spin part, $\langle j_0 \rangle$, was considered and for R^{3+} the dipolar approximation was used for calculating c_2.

Experimental results

Structural refinements

The crystallographic structures of R_2BaNiO_5 at room temperature have been discussed in a previous report where a comparative study of the structural parameters upon the rare earth size was performed [6]. In the present work, the dependence of these parameters with the temperature has been studied. Table 1 gives the value of the thermal expansion coefficients fitting a linear polynomial function, $p(T) = p_0 + \alpha_p T$ (p = structural parameter), between room temperature and 20 K for the cell parameters. We can observe that the thermal expansion is highly anisotropic: the a-axis is almost constant or with a slightly negative thermal expansion coefficient, whereas b and c-axes show a positive linear dependence on temperature. It is worth remarking that in the Tb, Ho and Tm

Table 1. Thermal expansion coefficients of cell parameters, Ni-O distances and the angle O(1)-Ni-O(1) in the NiO_6 octahedra. These compounds crystallise in S.G. Immm with the atoms in the following special positions: $R(4j)(1/2, 0, z)$ $z \approx 0.202$; $Ba(2c)(1/2, 1/2, 0)$; $Ni(2a)(0, 0, 0)$; $O(1)(8l)(0, y, z)$ $y \approx 0.24$, $z \approx 0.147$; O(2) (2b) (1/2,0,0). The structural parameters p as a function of T are obtained from the expression $p(T) = p_0 + \alpha_1 T$, with T in kelvin. The disparity in the standard deviation of the parameters reflects the different quality of the data.

		Nd	Tb	Dy	Ho	Er	Tm
a-axis	p_0	3.8249(8)	3.7837(2)	3.7622(8)	3.7545(4)	3.7446(7)	3.742(1)
	α_1	≈ 0	$-3.7(6) \times 10^{-5}$	$-8(2) \times 10^{-6}$	$-8(2) \times 10^{-6}$	$-6.5(4) \times 10^{-5}$	$-1.9(2) \times 10^{-4}$
b-axis	p_0	5.9068(1)	5.7811(3)	5.7403(1)	5.7321(4)	5.7251(7)	5.6861(2)
	α_1	$5(5) \times 10^{-6}$	$3.5(7) \times 10^{-5}$	$2.6(4) \times 10^{-5}$	$3.2(2) \times 10^{-5}$	$1.1(4) \times 10^{-5}$	$1.9(2) \times 10^{-4}$
c-axis	p_0	11.6051(2)	11.3881(5)	11.2821(4)	11.2711(1)	11.267(2)	11.2011(4)
	α_1	$3.2(6) \times 10^{-5}$	$2(1) \times 10^{-5}$	$2(1) \times 10^{-5}$	$8.5(5) \times 10^{-5}$	$9.8(9) \times 10^{-5}$	$4(4) \times 10^{-5}$
Ni-O(2)	p_0	1.9125(4)	1.8918(1)	1.8811(5)	1.8773(2)	1.8723(3)	1.8709(7)
	α_1	$-1(1) \times 10^{-6}$	$-1.8(3) \times 10^{-5}$	$-4(1) \times 10^{-6}$	$-4.7(9) \times 10^{-6}$	$-3.2(2) \times 10^{-5}$	$-8.6(9) \times 10^{-5}$
Ni-O(1)	p_0	2.220(2)	2.19(5)	2.194(3)	2.1792(2)	2.189(3)	2.163(2)
	α_1	≈ 0	≈ 0	$1.1(9) \times 10^{-4}$	$1.49(6) \times 10^{-5}$	$4(5) \times 10^{-5}$	≈ 0
O-Ni-O	p_0	81.2(1)	78.7(4)	83.5(2)	78.716(1)	79.03(6)	78.1(2)
	α_1	≈ 0	$3.1(1) \times 10^{-2}$	$7(6) \times 10^{-3}$	$-1.1(3) \times 10^{-2}$	$3.8(3) \times 10^{-2}$	≈ 0

cases the *a*-axis (chain direction) shows a tiny discontinuity close to the ordering temperature, certainly related with the 3D-AF ordering and the accompanying magnetostriction effects [11]. As an example we present in Figure 1 the temperature dependence of the cell parameters of the Nd compound.

In our previous structural work [6] we were interested in the variation of the NiO_6 octahedra as a function of the rare earth ionic size. As a matter of fact its volume varies linearly with the size of the rare earth ions, indicating that the chemical pressure is nearly hydrostatic in this family of compounds. Here we give the temperature dependence of some relevant structural parameters. The data gathered in Table 1 show that the distance Ni-O(2) = $a/2$ along the chain follows closely the variation of the *a*-axis with negative thermal expansion coefficient. The distance Ni-O(1) in the basal plane is almost constant, only in Nd case show a negative linear dependence with the temperature. Another important point is that the angle O(1)-Ni-O(1) ($\approx 78°$) in the basal plane remains almost constant within the error bars. However this angle in the Ho compound presents a dependence on temperature from T_N to 33 K, being almost constant from 33 K to 1.5 K [11]. By contrast the thermal expansion of the polyhedral environment of Ba and R is negligible from 1.5 K to 70 K. This is specially striking because Ba-O bonds are normally much softer than R-O or Ni-O bonds.

General features of the magnetic ordering

Below the Néel temperature all the observed Bragg peaks were indexed within a commensurate lattice related to the crystallographic cell (Immm) by a propagation vector $\mathbf{k} = (1/2, 0, 1/2)$ (the components are referred to the reciprocal vectors of the conventional unit cell). The $k_x = 1/2$ is clearly expected from the strong Ni-O-Ni AF superexchange interaction, but the other components of $\mathbf{k}$ should be explained from the whole set of exchange interactions existing in these compounds.

As an example of the typical diffraction patterns obtained at low temperature, in Figure 2 it is shown
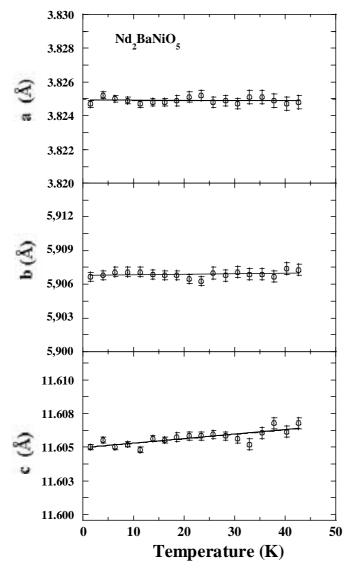
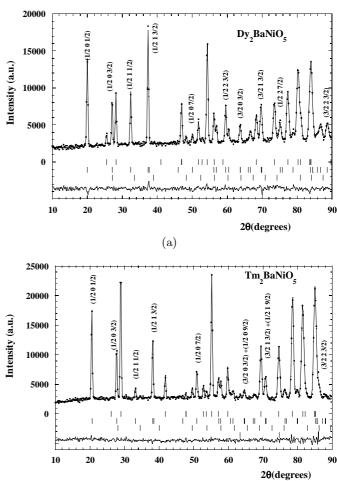Fig. 1. Variation of the lattice parameters a, b and c with temperature of Nd_2BaNiO_5 compound.

Fig. 2. Neutron diffraction pattern of Dy_2BaNiO_5 and Tm_2BaNiO_5 at 1.5 K. Vertical marks correspond to the position of the allowed Bragg reflections for the crystallographic (first row) and magnetic (second row) of the main phase. The third and fourth row corresponds to the Bragg reflection positions of the R_2O_3 impurities and NiO respectively.
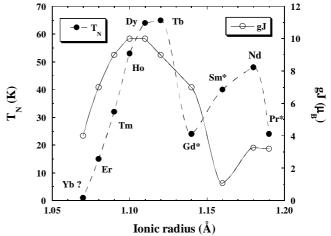

Fig. 3. The Néel temperature of the R_2BaNiO_5 and the gJ value of R^{3+} vs. rare earth ionic radius. Data for Gd and Sm are obtained from magnetic susceptibility. Data for Pr are from [12].

the observed and calculated patterns of Dy_2BaNiO_5 and Tm_2BaNiO_5 at 1.5 K.

The temperature evolution of the magnetic Bragg peaks allows the determination of the Néel temperature. Figure 3 shows the dependence of the Néel temperature of these compounds versus the ionic radius of the rare earth. We observe a linear behaviour for the heaviest rare earth ions (Tm-Dy) and after that, the curve diminishes for the largest rare earth ions. We observe a large reduction in the ordering temperature for Gd compound. This value and that of the Sm compound was obtained from magnetic susceptibility measurements because of the large absorption cross-section of Gd and Sm for thermal neutrons, so their T_N are uncertain. The Gd compound is interesting because the spin-only contribution to the magnetic moments ($L = 0$) and the anisotropy due to crystal field effects are absent in first approximation.

Table 2. Irreducible representations of the wave vector group $G_{0\mathbf{k}}(2/m)$, with $\mathbf{k} = (1/2, 0, 1/2)$ of $G = $ Immm.

	E	m_y	2_y	i
A_g	1	1	1	1
B_g	1	−1	−1	1
A_u	1	−1	1	−1
B_u	1	1	−1	−1

Table 3. Basis vectors for the R and Ni sublattices.

	R			Ni		
	x	y	z	x	y	z
$\Gamma^1(A_g)$	-	F_y	-	-	S_y	-
$\Gamma^2(B_g)$	F_x	-	F_z	S_x	-	S_z
$\Gamma^3(A_u)$	A_x	-	A_z	-	-	-
$\Gamma^4(B_u)$	-	A_y	-	-	-	-

In the same figure is shown the free ion magnetic moment of the rare earth.

The classification of the possible magnetic structures based on group theory

In order to determine the magnetic structures we have performed the symmetry analysis as described in [19,20]. The symmetry operations of the high temperature space group $(T > T_N)$, which keep invariant the propagation vector, (or transforms it into an equivalent vector differing by an arbitrary reciprocal lattice vector) form the wave vector group $G_{\mathbf{k}}$. In our case, we have $G_{\mathbf{k}}/T = \{E, m_y, 2_y, i\}$ where T is the invariant translation subgroup. In the case of a centred lattice, T is constituted by translations of the form $\mathbf{R}_n = n_1\mathbf{a} + n_2\mathbf{b} + n_3\mathbf{c}$ or $\mathbf{R}_n + \mathbf{t}_I$, where the centering translation is $\mathbf{t}_I = 1/2\mathbf{a} + 1/2\mathbf{b} + 1/2\mathbf{c}$. We shall use the index "n" for whatever lattice point irrespective of the type of translation.

Because $G_{\mathbf{k}}$ is a symmorphic group the irreducible representations are obtained from those of its point group $G_{0\mathbf{k}}$. The group $G_{0\mathbf{k}} = 2/m$ is commutative, so its irreducible representations are one dimensional. Table 2 gives the characters/matrices of the irreducible representations Γ^ν of $G_{0\mathbf{k}}$.

The irreducible representations of the entire space group G are specified by the star of the wave vector $\mathbf{k}$, which is a set of non-equivalent wave vectors obtained by the application of all the symmetry elements of the point group G_0, and the representations of $G_{\mathbf{k}}$ through the induction formula. In our case the star has two arms, constituted by the propagation vectors $\mathbf{k}_1 = (1/2, 0, 1/2)$ and $\mathbf{k}_2 = (1/2, 0, -1/2)$. The magnetic moment, $\mathbf{S}_{n,j}$, of the atom "j" attached to the lattice point $\mathbf{R}_n$ for a magnetic structure described by a set $\{\mathbf{k}\}$ of propagation vectors can be written as a Fourier series:

$$\mathbf{S}_{nj} = \sum_{\{\mathbf{k}\}} \mathbf{S}_{\mathbf{k},j} \exp\{-2\pi i \mathbf{k} \mathbf{R}_n\}, \tag{1}$$

where the Fourier coefficients $\mathbf{S}_{\mathbf{k},j}$ can be identified with the magnetic moments only in the case of a single propagation vector of the form $\mathbf{k} = 1/2\mathbf{H}$, being $\mathbf{H}$ a reciprocal lattice vector. Within the hypothesis of constant modulus of magnetic moments ($|\mathbf{S}_{n,j}| = |\mathbf{S}_{m,j}|$), the magnetic structure should be described either with a single propagation vector or $\mathbf{S}_{\mathbf{k}_1,j}$ must be perpendicular to $\mathbf{S}_{\mathbf{k}_2,j}$. We shall consider in the following that only one propagation

vector $\mathbf{k} = \mathbf{k}_1$ defines the magnetic structure, then the Fourier component $\mathbf{S}_{\mathbf{k},j}$ can be identified with the magnetic moment of the atom "j", $\mathbf{S}_j$, in the reference cell.

The Ni ions are in a single Bravais sublattice at $(000)(2a)$ site. The rare earth site $(4j)$ generates two sublattices 1: $(1/2, 0, z)$ and 2:$(-1/2, 0, -z)$ in a primitive unit cell, with magnetic moment components $S_{i\alpha}$, being $i = 1, 2$ and $\alpha = x, y, z$. The rest atoms of the conventional unit cell are related to those already given by the centering translation $\mathbf{t}_I$. The magnetic moment in positions outside the reference cell are calculated from those at the reference cell by the expression (1). Thus, in order to describe the magnetic structure we need to know only the magnetic moment components of the Ni ion at the origin and the magnetic moment components of R_1 at $(1/2,0,z)$ and R_2 at $(-1/2, 0, -z)$.

From the transformation properties of the R spin vectors we generate a reducible representation $\Gamma(R)$ of $G_{\mathbf{k}}$. The four transformation matrices of the four symmetry operations $\{E, m_y, 2_y, i\}$ in the space of $S_{i\alpha}$ components, have dimension 6×6 and their traces are $(6, -2, 0, 0)$.

In the case of Ni, only one atom located at $(0, 0, 0)$ with magnetic components S_α $(\alpha = x, y, z)$ generate the whole sublattice. The dimension of the representative matrices is 3×3, and their traces are $(3, -1, -1, 3)$ for the same symmetry operations. By the application of standard formulae, the irreducible representations contained in $\Gamma(R)$ and $\Gamma(Ni)$ are:

$$\Gamma(R) = A_g + 2B_g + B_u + 2A_u$$
$$\Gamma(Ni) = A_g + 2B_g.$$

Following the Bertaut method, only vectors belonging to the same representation of both sites (R and Ni) may be coupled [19], in first approximation. Thus, we have to consider first the even representations A_g and B_g as the candidates to describe the magnetic structures.

To write the basis functions in a compact form, we define the following two magnetic modes for the R atoms in a primitive cell: $\mathbf{F} = \mathbf{S}_1 + \mathbf{S}_2$ and $\mathbf{A} = \mathbf{S}_1 - \mathbf{S}_2$. Using the projection operator formula it is straightforward to obtain the basis functions presented in Table 3 for the $R_{1,2}$ and Ni sublattices.

The simplicity of the crystal structure allows us writing up an explicit formula for the magnetic intensity of single reflection informing about the possible existence of physically different solutions giving rise to the same powder diffraction pattern. For the scattering vector $\mathbf{Q} = 2\pi(\mathbf{H}+\mathbf{k}) = 2\pi(h+1/2, k, l+1/2)$, the magnetic intensity

Table 4. Magnetic structural parameters of R_2BaNiO_5 compounds. The magnetic moments of R^{3+} and $Ni^{2+}(R)$ are given at 1.5 K, in Cartesian and spherical co-ordinates.

	T_N	Γ	$\mu(\mu_B)$	ϕ	θ	S_x	S_y	S_z	$gJ(\mu_B)$
Pr [12]	24	B_g	1.3		0			1.3	3.2
Ni		B_g	1.1		0			1.1	2
Nd	48	B_g	2.65(2)		−0.9	−0.05		2.65(2)	3.27
Ni		B_g	1.6(1)		143(7)	0.9(3)		−1.30(7)	2
Tb	65	B_g	8.03(4)		4.9(4)	0.68(6)		8.00(4)	9
Ni		B_g	2.01(8)		132(2)	−1.5(1)		−1.35(5)	2
Dy	64	B_g	7.7(5)		0.45	0.06(9)		7.70(5)	10
Ni		B_g	1.3(1)		17(8)	0.4(2)		1.29(7)	2
Ho	53	B_g	9.06(4)		0.7(3)	0.12(5)		9.06(4)	10
Ni		B_g	1.41(5)		154(4)	0.58(9)		−1.26(4)	2
Er	32	B_g	7.24(5)		87.5(5)	7.23(5)		0.32(6)	9
Ni		B_g	1.39(6)		83 (4)	1.38(6)		0.18(9)	2
Tm	15	$B_g + A_g$	3.34(4)	101(6)	98(8)	−0.6(2)	3.24(7)	−0.5(4)	7
Ni		$B_g + A_g$	1.2(1)	285(30)	83(40)	0.3(5)	−1.1(1)	0.14(5)	2

is proportional to the square of the perpendicular to $\mathbf{Q}$ component of the magnetic structure factor vector:

$$\mathbf{F}_m(\mathbf{H} + \mathbf{k}) = \mathbf{S}\, f_{Ni}(\mathbf{Q})\, e^- W_{Ni} + e^- W_R f_R(\mathbf{Q})$$
$$\times \{\mathbf{S}_1 \exp[i\mathbf{Q}\, \mathbf{r}_1] + \mathbf{S}_2 \exp[i\mathbf{Q}\, \mathbf{r}_2]\}$$

$$= \mathbf{m} + i(-1)^h\{\mathbf{m}_1 \exp[\pi i\, z(2l + 1)]$$
$$- \mathbf{m}_2 \exp[-\pi i\, z(2l + 1)]\} \cdot \qquad (2)$$

The symbols following usual conventions and the last equality defining the **m**-vectors. From Table 3 there is no mixture of modes A and F within an irreducible representation for the R sublattices, then $\mathbf{m}_2 = \mathbf{m}_1$ (F-mode) or $\mathbf{m}_2 = -\mathbf{m}_1$ (A-mode) for all cases. Taking the perpendicular components $\mathbf{m}_\perp = \mathbf{e} \times \mathbf{m} \times \mathbf{e}$, with $\mathbf{e} = \mathbf{Q}/Q$, one obtains:

$$\mathbf{F}_{\perp(F)} = \mathbf{m}_\perp + 2(-1)^{h+1}\, \mathbf{m}_{\perp 1} \sin[\pi z(2l + 1)] \qquad (3)$$
$$\mathbf{F}_{\perp(A)} = \mathbf{m}_\perp + 2i(-1)^h\, \mathbf{m}_{\perp 1} \cos[\pi z(2l + 1)]. \qquad (3')$$

The intensity is given by:

$$I_F(\mathbf{H} + \mathbf{k}) \approx m_\perp^2 + 4m_{\perp 1}^2 \sin^2[\pi z(2l + 1)]$$
$$+ 4(-1)^{h+1}\, \mathbf{m}_\perp \cdot \mathbf{m}_{\perp 1} \sin[\pi z(2l + 1)] \qquad (4)$$

$$I_A(\mathbf{H} + \mathbf{k}) \approx m_\perp^2 + 4m_{\perp 1}^2 \cos^2[\pi z(2l + 1)]$$
$$+ 4(-1)^h\, \mathbf{m}_\perp \cdot \mathbf{m}_{\perp 1} \cos[\pi z(2l + 1)]. \qquad (4')$$

From the expressions (4) and (4') and from the orthorhombic symmetry of the compounds it is easy to see that there is no ambiguity for distinguishing the different modes and the absolute orientations of the magnetic moments (except for a whole inversion) even with powder samples. The only ambiguity could come from the nature single or double-**k** type of the structure which cannot be determined, in general, from powder samples due to the perfect superposition of independent sets of reflections. The basis functions of the double-**k** structure (restoring the full orthorhombic magnetic symmetry) give non-constant-moment magnetic arrangements and, as expected, we obtained a good fit of the experimental data with a non-constant-moment structure in the Ho case. However, there is no physical reason to accept such a kind of magnetic structure in these materials and we shall consider that we are in presence of a single-**k** magnetic structure for the whole set of studied compounds.

Magnetic structure determination and refinement

The magnetic structures are summarised in Table 4. From Nd to Er the best fit to the experimental data is obtained for the B_g representation. The relationship between the two magnetic moments is $S_{2x} = S_{1x}$, $S_{2y} = S_{1y} = 0$, $S_{2z} = S_{1z}$. In the case of the Ni sublattice the two basis vector are directly the x and z components of the magnetic moment. This means that the Ni and R-moments are within the ac-plane. In the Tm case the use of the basis functions of the reducible representation
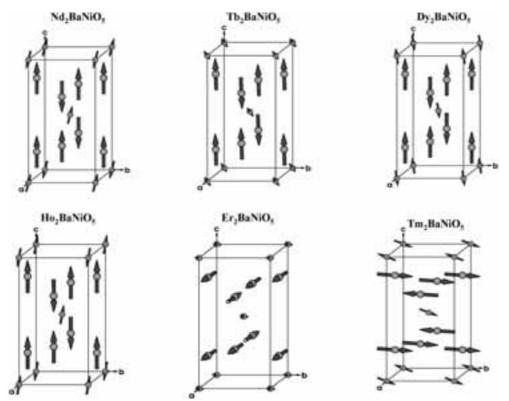
Fig. 4. Representation of the family R$_2$BaNiO$_5$ magnetic structures at 1.5 K. Only one crystallographic unit cell is shown.

$G_{Tm} = A_g + 2B_g$ was necessary to obtain a good refinement. The coupling between the Tm-moment components is: $S_{2x} = S_{1x}$, $S_{2y} = S_{1y}$, $S_{2z} = S_{1z}$ and S_x, S_y, S_z for Ni sublattice. Then there is no spatial restriction for the directions of Ni and Tm-moments. The mixture of two irreducible representations for describing a magnetic structure is not very common, but about 10% of the magnetic structures described in [21] present this feature. The mixing of different irreducible representations is related to the weakness of the magnetic anisotropy (see discussion about "exchange multiplets" in [20]) that should be much lower in the Tm compound than in the other studied rare earth compounds.

Table 4 summarises the magnetic moment components of the representative atoms of R^{3+} and Ni^{2+} at 1.5 K. The magnetic moments are written in Cartesian components (S_x, S_y, S_z) as well as in spherical co-ordinates (μ, ϕ, θ). The main result is that the magnetic moments of Nd, Tb, Dy and Ho are nearly aligned along the c-axis, perpendicular to the NiO$_6$ chains. In these compounds, Ni-magnetic moments form relative small angles with the c-axis. The value of the magnetic moment of R^{3+} is close to the expected value for the free ion R^{3+}, except for Tm^{3+} where a strong magnetic moment reduction from the free ion value ($gJ = 7\mu_B$) is observed. In the case of Ni the averaged magnetic moment is 1.4 μ_B. This value is lower than that expected for Ni^{2+} (2 μ_B). Even in nearly 2D-systems like La$_2$NiO$_4$, with Ni^{2+} in octahedral co-ordination, the saturation moment is close to 1.5 μ_B, being explained this reduction by covalency effects and quantum spin fluctuations in 2D [1]. In this family 1.4 μ_B represents a stronger

reduction probably due to the strong covalency related to the very unusual short apical distance of 1.88 Å.

In order to refer the Ni sublattices in the different compounds we shall use the short symbol "Nickel (rare earth)". For example, Ni(Tm) means the Nickel sublattices in the Tm$_2$BaNiO$_5$ compound.

As in the Ho$_2$BaNiO$_5$ case, where the Ni-moments form an angle of 26° respect the negative direction [001], the Ni(Nd) and Ni(Tb) moments form an angle of 37° and 48° respectively, with the same negative direction. As contrast, in Ni(Dy) case this angle is 17° in the positive direction [001]. It is interesting to compare these results with those obtained for Er$_2$BaNiO$_5$. The Er-magnetic moments are almost parallel to the chains (a-axis). Ni(Er) moments are aligned an angle of 7° with the positive direction [100]. At variance with all compounds of this family, the Tm and Ni(Tm) magnetic moments are not restricted to the ac plane, *i.e.* there is also a component along b, because of the mixing of two irreducible representations. In Table 4 we show that Tm-magnetic moment is nearly aligned along the b-axis, forming an angle of 11° with the positive direction [010]. Ni(Tm) is mainly pointing along the $[0\bar{1}1]$ direction with a small a-component. The projection of Ni(Tm) moment on the ab plane forms an angle of 15° with the negative direction [010].

The different directions of the magnetic moments in these compounds reflect the magnetic anisotropy of the rare earth ions. A representation, by means of the program MAG3D [22] of all magnetic structures observed in this family is shown in Figure 4.
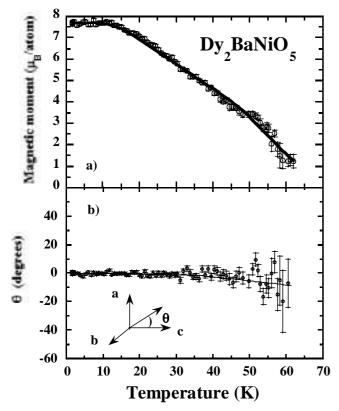
Fig. 5. Temperature dependence of a) the Dy^{3+} magnetic moment and b) θ angle, as defined in the inset. The continuous curve in (a) correspond to the mean-field model discussed in [16], in (b) the continuous curve is a guide to the eyes.

Temperature dependence of the magnetic structure

Let us now discuss the results obtained in the study of the thermal evolution of the magnetic moments in R_2BaNiO_5. The data concerning the magnetic structural parameters are represented as obtained from automatic sequential Rietveld refinements, so the instability of the algorithm approaching the Néel temperature gives rise to some outlier points. In the case of the amplitude of the magnetic moments of Ni^{2+} it was not possible to refine reliable values close to the Néel temperature. We have represented only the points giving stable refinement even if the standard deviations are large.

The continuous curves in the following figures fit qualitatively the experimental values of the magnetic moments and they correspond to the mean-field model discussed previously in our description of the macroscopic magnetic properties of this family of compounds (see Eqs. (1) and (4) of reference [16]). Continuous curves fitting the evolution of orientation angles are guides for the eyes.

Figure 5a shows the temperature dependence of the Dy^{3+} magnetic moment. In Figure 5b it is depicted the variation of the spherical θ angle with temperature. The error bars around the ordering temperature become important due to the small ordered moment.

The same thermal evolution was found for the largest rare earth ions (Nd, Tb, Dy, and Ho). The main result is
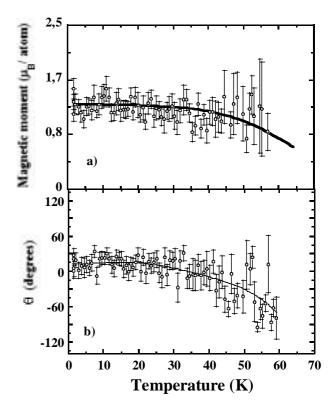

Fig. 6. Temperature dependence of a) Ni(Dy) magnetic moment, b) θ angle. The continuous curves are as in Figure 5.

that the value of the magnetic moment is close to the free ion value, and is almost fully aligned parallel to the c-axis ($\theta \approx 0°$) for Tb, Dy and Ho, due to the anisotropy of these ions and the high magnetic moment value. At variance, Nd ions seem to have the same preference anisotropic direction but the thermal evolution of the θ angle shows an increase of its value toward [$\bar{1}$00] direction.

In Figure 6a it is represented the magnetic moment of Ni^{2+} (Dy) *vs.* temperature showing that the ordering temperature is the same than that of the Dy sublattice. The Ni magnetic moment in all compounds increases rapidly and reaches its saturation temperature at a higher value than for the rare earth sublattices. In Figure 6b is shown the temperature dependence of the θ angle of the reference Ni(0,0,0) atom. Our results suggest that close to T_N the Ni(Dy, Ho) starts to be ordered with the magnetic moments pointing mainly along the NiO_6 chain. Just below, but close to T_N, the Ni moments start to rotate toward the c-axis, forced by the combination of the increasing ordered moment on the R site, the exchange Ni-R integrals and the anisotropy of the R^{3+} due to crystal field. At lower temperature, the Ni moment is mostly aligned along the c-axis with a small component parallel to the a-axis.

It is interesting to point out that for the Tb and Nd cases, the Ni(Tb, Nd) moments decrease rotating toward smaller angles with c-axis, *i.e.* close to ordering temperature the magnetic moments are pointing along the c-axis.

At variance with the rest of rare earths, the magnetic moments of Er^{3+} ions in the saturation temperature range are almost parallel to the chains (a-axis). The study of the
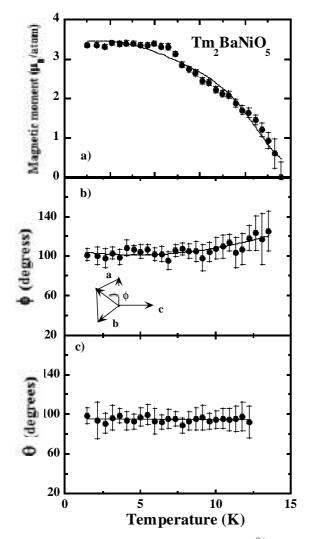
Fig. 7. Temperature dependence of a) the Tm^{3+} magnetic moment and b) ϕ angle, as defined in the inset c) θ angle. The continuous curves and θ angle as defined in Figure 5.
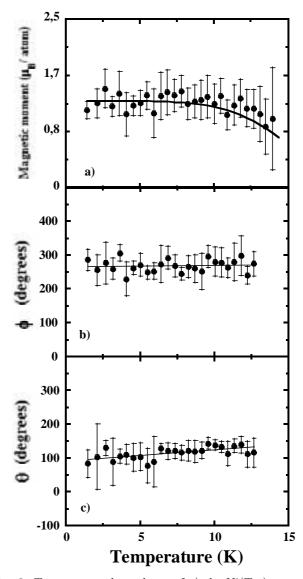

Fig. 8. Temperature dependence of a) the Ni(Tm) magnetic moment and b) ϕ angle and c) θ angle. The continuous curves are as in Figure 5.

thermal evolution of Ni and Er magnetic moments shows that the Ni(Er) moment decreases without changing the direction in the whole temperature range. The thermal behaviour of the Er moments indicate a small rotation ($\approx 10°$) towards the c-axis. Close to T_N, but the main Er-magnetic moment component remains along the a-axis.

As discussed above, the magnetic structure of Tm compound has no constraint on the magnetic moment direction, however the magnetic moment of Tm^{3+} is almost fully aligned along the b-axis, *i.e.* perpendicular simultaneously to the chains and to the c-axis which is the main magnetic moment direction for the rare earth ions with the largest moments. Due to the difference of the magnetic structure with the rest of the family, we include in Figure 7 and Figure 8 the temperature dependence of the three spherical co-ordinates (μ, ϕ, θ). We can observe that the moment direction is almost constant, within the error bars.

Discussion

The family of compounds R_2BaNiO_5 presents maxima in the magnetic susceptibility, which are always at much lower temperatures that the 3D-AF ordering temperatures (T_N) observed by neutron diffraction [14,15]. For instance, in Er_2BaNiO_5 the temperature of the maximum is $T_{Max} \approx 16$ K and $T_N \approx 33$ K; for Ho_2BaNiO_5 $T_{Max} \approx 33$ K and $T_N \approx 53$ K [15,16]. However, our data from the study of the magnetic susceptibility by SQUID magnetometry show two anomalies at different temperatures: a broad maximum and an extra peak [15,16]. This peak determines a transition temperature coinciding with that observed by neutron diffraction and a simplified molecular field model, proposed first by Chepurko *et al.* [15], explains the presence of a broad maximum below the Néel temperature.

The dependence of the order temperature of this family *versus* the ionic radius (Fig. 3) suggests the influence of the volume, as well as the value of gJ, in the magnetic order. As we reported previously [6], the rare earth size influences on the structural parameters in a linear way. The ordering temperature follows a similar behaviour for the smallest rare earths, *i.e.* T_N increases linearly from Yb to Dy. For Tb is slightly higher than for Dy and for larger R^{3+} decreased suddenly for the Gd compound. That indicates that the anisotropy of the rare earth ions also contributes to reach the magnetic order at higher temperatures.

It is important to mention that Yb_2BaNiO_5 does not present magnetic order above 1.5 K. *A priori*, there is not reason for this feature because all this family present the same crystal structure, due to this fact the pathways for the interactions should be the same. However, as we mentioned above, the role of the rare earth size as well as the intrinsic magnetic moment is critical to observe the 3D magnetic order. In the assumption of the linear dependence of the ordering temperature for the smallest rare earth ions, the extrapolated Néel temperature value of Yb_2BaNiO_5 is 0.7 K. Our data were collected above 1.5 K.

Neutron diffraction patterns of Y_2BaNiO_5 at low temperature corroborate the absence of 3D magnetic ordering. At variance with Yb_2BaNiO_5, the origin of this behaviour can be clearly explained: the chains are magnetically isolated, being linked through the diamagnetic Y^{3+} and Ba^{2+} cations. Because of that, the magnetic inter-chain interactions are weak and the 3D magnetic ordering is not observed. The ground state is then non-magnetic as predicts the Haldane's conjecture about $S = 1$ spin chains. Thus, we can assume that the superexchange interactions between rare earth and nickel sublattices play a key role on the magnetic order of R_2BaNiO_5 (R = paramagnetic ion) compounds.

As in the case of the Y-compound, R_2BaNiO_5 should present strong 1D-AF correlations well above room temperature. It is quite probable that these correlations have a fluctuating character in time, so that no static 1D ordering exist. The 1D-AF correlations are very difficult to observe from magnetic susceptibility due to the important paramagnetic moment from the R ions. In neutron diffraction quasi-static 1D-AF ordering does not produce any Bragg peak. Near, but above, T_N quasi-static short-range ordering is observed for Ho_2BaNiO_5 and Tb_2BaNiO_5. The diffuse scattering up to $T_N + 10$ K is likely due to the Ni-R interactions, which are responsible of the coupling between different chains, establishing the short-range ordering.

Zheludev and co-workers [23,25], have performed a series of inelastic-neutron-scattering experiments demonstrating that the Haldane's type of excitation (around 11 meV in the 1D AF zone centre for these compounds) persist above and below T_N in both the Nd and Pr compounds. The gap increasing on cooling below T_N. The quantum nature (related to the $S = 1$ Ni^{2+} chains) of this excitation seems to be clear, but it is expected that for heavier rare earths normal spin waves and rare earth crystal field transitions will dominate the magnetic excitation spectrum in these family of compounds.

It is interesting to remark the shape of the curve representing the amplitudes of the magnetic moment of the rare earth *vs.* temperature. At the lowest temperature we found the a saturated magnetic moment value that, as the temperature increases, starts to diminish nearly linearly to reach the ordering temperature. The overall shape can be explained by a simple molecular field model taking into account the Ni-Ni and Ni-R interactions [15,16,24].

One of the problems remaining to be treated, from the point of view of the magnetic ground state of this family, is the identification of the exchange interactions that are responsible for the propagation vector $\mathbf{k} = (1/2, 0, 1/2)$. In the following we shall demonstrate that R-Ni interactions alone cannot explain the component $k_z = 1/2$ in the ground state wave vector. We shall assume that the propagation vector of the classical ground state correspond to a minimum of the magnetic energy [26] given by:

$$E = -\sum J_{ij} \mathbf{S}_i \cdot \mathbf{S}_j \qquad (5)$$

where $\mathbf{S}_i$ is considered as a classical spin at site "i" interacting with the spin at site "j" through the exchange integral J_{ij}. The consideration of anisotropic exchange, single ion anisotropy, dipolar, or higher order (biquadratic for instance) spin interactions will not change our conclusions provided they are weak compared with the isotropic exchange. This is so if we consider, as is the common belief in insulators, that the isotropic exchange, between the spins of two not too far away atoms, is the most important term responsible for the magnetic ordering. The minimisation of (5) with the constraint of constant magnetic moments at $T = 0$ is, in general, a complicated problem [26] but in our case there is no magnetic phase transition and we can assume that the first magnetic order state (just below T_N) is the same (except for the value of the magnetic moments) as the ground state. This is exact in what concerns the propagation vector. The first magnetic order state can be calculated from the generalisation of the Villain's theorem for Bravais lattices [26]. This state correspond to the maximum eigenvalue of the Fourier transform matrix of exchange interactions:

$$J_{ij}(\mathbf{k}) = \sum J_{ij}(\mathbf{R}_0 - \mathbf{R}_n) \exp\{-2\pi i \, \mathbf{k} \, \mathbf{R}_n\} \cdot \qquad (6)$$

Now the subscripts "i" and "j" labels atom positions inside the primitive unit cell. The exchange interactions in (6) include the products of the modules of the magnetic moments of the atoms "i" and "j". In our case we have three atoms (1 Ni and 2 rare earths) in the primitive cell. In Figure 9 we have represented the exchange interactions considered in our model.

J_1 is the 180° Ni-O(2)-Ni superexchange interaction along the chain and it is the strongest exchange integral in the structure. J_2 is the nearest-neighbour 90° Ni-O(2)-R interaction and it is expected to be small. J_3 is the next-nearest-neighbour $\approx$180° Ni-O(1)-R interaction and it is expected to be the strongest Ni-R interaction. J_4 is the R-R exchange along the chain, J_5 is the nearest-neighbour R-R direct exchange and they are expected to be very weak. The last R-R interaction considered here, J_6, is the
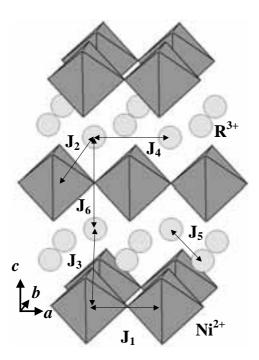
Fig. 9. Scheme of the exchange interactions paths described in the text.

180° superexchange R-O(1)-R, in a path perpendicular to the chains. With this notation, using $\mathbf{k} = (X, Y, Z)$ in reciprocal lattice units and restricted to the first Brillouin zone, the terms of the matrix (6) for our case are:

$$J_{11}(\mathbf{k}) = 2J_1 \cos 2\pi X$$

$$J_{12}(\mathbf{k}) = J_{21}(\mathbf{k})^* = J_2(1 + \exp\{2\pi i X\}) \\ + 2J_3 \cos \pi Y \exp\{\pi i (X + Z)\}$$

$$J_{13}(\mathbf{k}) = J_{31}(\mathbf{k})^* = J_2(1 + \exp\{2\pi i X\}) \exp\{2\pi i Z\} \\ + 2J_3 \cos \pi k \exp\{\pi i (X + Z)\}$$

$$J_{22}(\mathbf{k}) = J_{33}(\mathbf{k}) = 2J_4 \cos 2\pi X$$

$$J_{23}(\mathbf{k}) = J_{32}(\mathbf{k})^* = 4J_5 \cos \pi X \cos \pi Y \exp\{\pi i Z\} \\ + J_6 \exp\{2\pi i Z\} \cdot$$

The general expression of the eigenvalues of the matrix is quite cumbersome. If we make some simplifications we can gain insight into the problem of the classical ground state of these systems. If we neglect all R-R interactions we obtain a simple expression for the eigenvalues as a function of $\mathbf{k}$:

$$\lambda_1(\mathbf{k}) = 0, \lambda_{2,3}(\mathbf{k})$$
$$= 2J_1 \cos 2\pi X \pm \left(J_1^2 \cos^2 2\pi X + 4J_3^2 \left\{1 + \cos^2 2\pi Y\right\}\right)^{1/2}.$$

It is clear that the energy of the ground state does not depend on the Z component of $\mathbf{k}$, so the ground state is infinitely degenerated if R-R interactions are neglected. The 3D magnetic order cannot be attained if our compounds are considered as isotropic Heisenberg systems without R-R exchange interactions.

A detailed analysis of the magnetic phase diagram as a function of the exchange integrals is out of the scope of the present paper.

Final remarks and perspectives

The different magnetic moment directions in these compounds indicate that the single-ion anisotropy plays an important role. Thus, the single-ion anisotropy of R^{3+} in Nd, Tb, Dy and Ho compounds favours clearly the orientation of the magnetic moments along the c-axis, while the single-ion anisotropy of Er^{3+} favours the alignment along the a-axis. In the case of Tm, the anisotropy should be much smaller as suggested by the magnetic structure that should be described by the mixing of two irreducible representations: the orientation of the magnetic moments of Tm is in a general direction but with the main component along b. An inelastic-neutron-scattering experiment is needed to determine the crystal field excitations that may help to calculate the preference direction in the ground state.

According to Chepurko *et al.* [15], the R_2BaNiO_5 (R = Nd, Gd, Tb, Dy, Ho, Er, Tm) oxides present two metamagnetic transitions at 4.2 K for magnetic fields between 13 kOe to 180 kOe. In the case of Ho_2BaNiO_5 these metamagnetic transitions are observed at 23 kOe and 33 kOe. However no good quality data, with the corresponding values of the magnetisation associated with each metamagnetic transition, are available yet. These transitions will be probably associated with changes in the propagation vector of the magnetic structure. A neutron diffraction experiment, using single crystals under applied magnetic field, is needed for determining the nature of the metamagnetic transitions. At present we do not dispose of crystals of sufficient size for performing such an experiment.

References

1. J.L. Martínez, M.T. Fernández-Díaz, J. Rodríguez-Carvajal, P. Odier, Phys. Rev. B **43**, 13766 (1991). See also J. Rodríguez-Carvajal, M.T. Fernández-Díaz, J.L. Martínez, F. Fernández, R. Sáez-Puche, Europhys. Lett. **11**, 261 (1990); J. Rodríguez-Carvajal, M.T. Fernández-Díaz, J.L. Martínez, J. Phys. Cond. Matt. **3**, 3215 (1991).
2. See references in J.M. Tranquada, J.E. Lorenzo, D.J. Buttrey, V. Sachan, Phys. Rev. B **52**, 3581 (1995).
3. J.L. García-Muñoz, J. Rodríguez-Carvajal, P. Lacorre, Phys. B **180/181**, 306 (1992). See also P. Lacorre, J.B. Torrance, J. Pannetier, A.I. Nazzal, P.W. Wang, T.C. Huang, R.L. Siemens, J. Solid State Chem. **91**, 225 (1991).
4. S.T. Schiffler, H.K. Müller-Buschbaum, Z. Anorg. Allog. Chem. **540/541**, 243 (1986).
5. J. Amador, E. Gutierrez-Puebla, M.A. Monge, I. Rasines, J.A. Campá, C. Ruiz-Valero, J.M. Gomez de Salazar, Solid State Ionics **32/33**, 123 (1989).

6. E. García-Matres, J.L. Martínez, J. Rodríguez-Carvajal, J.A. Alonso, A. Salinas-Sánchez, R. Sáez-Puche J. Sol. St. Chem. **103**, 322 (1993).

7. A. Salinas-Sánchez, R. Sáez-Puche, J. Rodríguez-Carvajal, J.L. Martínez, Solid State Commun. **78**, 481 (1991).

8. J. Darriet, L.P. Regnault Solid State Commun. **86**, 409 (1993).

9. Guangyong Xu, J.F. Ditusa, T. Ito, K. Oka, H. Takagi, C. Broholm, G. Aeppli, Phys. Rev. B **54**, 6827 (1996).

10. J.A. Alonso, J. Amador, J.L. Martínez, I. Rasines, J. Rodríguez-Carvajal, R. Sáez-Puche, Solid State Commun. **76**, 467 (1990).

11. E. García-Matres, J. Rodríguez-Carvajal, J.L. Martínez, A. Salinas-Sánchez, R. Sáez-Puche, Solid State Commun. **85**, 553 (1993).

12. A. Zheludev, J.M. Tranquada, T. Vogt, D.J. Buttrey, Europhys. Lett. **35**, 385 (1996).

13. V. Sachan, D.J. Buttrey, J.M. Tranquada, G. Shirane, Phys. Rev. B **49**, 9658 (1994).

14. J. Amador, E. Gutierrez-Puebla, M.A. Monge, I. Rasines, C. Ruiz-Valero, F. Fernández, R. Sáez-Puche, J.A. Campá, Phys. Rev. B **42**, 7918 (1990).

15. G.G. Chepurko, Z.A. Kazei, D.A. Kudrjautser, R.Z. Levitin, B.V. Mill, M.W. Popova, V.V. Snegirer, Phys. Lett. A **157**, 81 (1991).

16. E. García-Matres, J.L. Garcia-Muñoz, J.L. Martínez, J. Rodríguez-Carvajal, J. Magn. Magn. Mater. **149**, 363 (1995).

17. J. Rodríguez-Carvajal, Physica B **192**, 55 (1993).

18. P.J. Brown in *International Tables for Crystallography*, Vol. C, edited by A.J.C. Wilson (Kluwer Academic Publishers, London 1992).

19. E.F. Bertaut, Acta Cryst. A **24**, 217 (1968).

20. Y.A. Izyumov, V.E. Naish, R.P. Ozerov, *Neutron diffraction of magnetic materials*, Consultants bureau, New York (1991).

21. A. Olés, F. Kajzar, M. Kucab, W. Sikora, *Magnetic Structures determined by neutron diffraction* (Polska Akademia Nauk, Warszawa, 1976).

22. P.J. Brown, *Program MAG3D, Cambridge Crystallography Subroutine library* (unpublished).

23. A. Zheludev, J.M. Tranquada, T. Vogt, D.J. Buttrey, Phys. Rev. B **54**, 6437 (1996).

24. A. Zheludev, J.M. Tranquada, T. Vogt, D.J. Buttrey, Phys. Rev. B **54**, 7210 (1996).

25. A. Zheludev, J.P. Hill, D.J. Buttrey, Phys. Rev. B **54**, 7216 (1996).

26. M.J. Freiser, Phys. Rev. **123**, 2003 (1961).